Novel Lambda FRET Spectral Confocal Microscopy Imaging Method

DIEGO MEGÍAS,[1] RAQUEL MARRERO,[1] BORJA MARTÍNEZ DEL PESO,[2] MARÍA ÁNGEL GARCÍA,[1] JOSÉ-JAVIER BRAVO-CORDERO,[1] ARANZAZU GARCÍA-GRANDE,[1] ANDRÉS SANTOS,[2] AND MARÍA C. MONTOYA[1]*

[1]*Biotechnology Programme, Confocal Microscopy and Cytometry Unit, Centro Nacional de Investigaciones Oncológicas (CNIO), C/ Melchor Fernández Almagro 3, Madrid E-28029, Spain*

[2]*Department of Electronic Engineering, Biomedical Image Technology Lab, Universidad Politecnica de Madrid, ETSI Telecomunicacion, Madrid E-28040, Spain*

KEY WORDS FRET; spectral; microscopy; imaging; confocal; interaction

ABSTRACT We report a highly specific, sensitive, and robust method for analyzing fluorescence resonance energy transfer (FRET) based on spectral laser scanning confocal microscopy imaging. The lambda FRET (λFRET) algorithm comprises imaging of a FRET sample at multiple emission wavelengths rendering a FRET spectrum, which is separated into its donor and acceptor components to obtain a pixel-based calculation of FRET efficiency. The method uses a novel off-line precalibration procedure for spectral bleed-through correction based on the acquisition of reference reflection images, which simplifies the method and reduces variability. λFRET method was validated using structurally characterized FRET standards with variable linker lengths and stoichiometries designed for this purpose. λFRET performed better than other well-established methods, such as acceptor photobleaching and sensitized emission-based methods, in terms of specificity, reproducibility, and sensitivity to distance variations. Moreover, λFRET analysis was unaffected by high fluorochrome spectral overlap and cellular autofluorescence. The λFRET method demonstrated outstanding performance in intra- and intermolecular FRET analysis in both fixed and live cell imaging studies. *Microsc. Res. Tech. 72:1–11, 2009.*

INTRODUCTION

Fluorescence resonance energy transfer (FRET) is a process through which an excited fluorophore (donor) transfers its energy to a nearby light-absorbing molecule (acceptor). FRET is dependent on the proximity of both molecules, which must be within a range of 1–10 nm of each other, making this technique a unique tool to quantitatively analyze the molecular interactions with spatial and temporal resolution (Förster, 1965; Jares-Erijman and Jovin, 2003). Microscopy FRET imaging allows one to monitor the molecular interactions in space (i.e., localizing interactions within cells or tissues) and time (i.e., observing the formation and breakdown of molecular complexes within a live cell) (Wouters et al., 2001; Zhang et al., 2002).

FRET microscopy is usually based on the presence of two fluorescent species; donor and acceptor. When donor is excited it will either emit fluorescence with its characteristic emission wavelength (λ) (in case there is no transfer of energy) or (when FRET occurs), its excited energy will be transferred to the acceptor which will emit with its characteristic λ. Therefore, in the event of FRET the following changes will occur; donor fluorescence emission intensity decreases, fluorescence emission at wavelengths characteristic of the acceptor emission will appear, and the half life of excited donor is reduced. The various FRET measuring methods are based on the quantification of these changes and require different instrumental set ups; ranging from wide field or laser scanning confocal microscopes, to the costly and highly specialized fluorescence lifetime imaging (FLIM) systems. Intensity-based methods relying on measuring variations in fluorescence intensity include "acceptor photobleaching," which is the most commonly used method for analyzing FRET in fixed cells because of its simplicity, and "sensitized emission," which is extensively used to study intramolecular FRET in live cells by conventional wide field or confocal microscopy. However, these methods have intrinsic limitations; in particular, acceptor photobleaching is destructive and therefore not applicable to live cell studies, and sensitized emission-based methods are subject to variability because of their strong dependence on external controls, which introduce a high level of instability to the measure. Because of all these difficulties, a microscopy method that uses a simple and reliable correction procedure for analyzing quantitatively FRET, applicable to live cells is still missing. We therefore sought to develop a FRET analysis

Additional Supporting Information may be found in the online version of this article.

Abbreviations: CFP, cyan fluorescent protein; FLIM, fluorescence lifetime imaging; FRET, fluorescence resonance energy transfer; mRFP, monomeric red fluorescent protein; YFP, yellow fluorescent protein.

*Correspondence to: Maria C. Montoya, Confocal Microscopy and Cytometry Unit, Biotechnology Programme, Spanish National Cancer Research Center (CNIO), C/ Melchor Fernández Almagro 3, Madrid E-28029, Spain.
E-mail: mmontoya@cnio.es

Received 4 July 2008; accepted in revised form 25 July 2008

Contract grant sponsor: Fondo de Investigaciones Sanitarias; Contract grant number: FIS PI061839; Contract grant sponsor: Ministry of Science and Technology of Spain.

DOI 10.1002/jemt.20633

Published online 10 September 2008 in Wiley InterScience (www.interscience.wiley.com).

method that could overcome these problems and that could be sensitive enough to detect typically weak physiological interactions in live cell studies.

Spectral imaging comprises the acquisition of fluorescence images at multiple wavelengths, and is based on the capability of a microscope system to separate the light emitted from the excited sample into its spectral components and collect them separately. This tool has been implemented in most standard laser scanning confocal microscopes currently available (Lerner and Zucker, 2004; Zimmermann et al., 2003), and provides a unique capability for monitoring changes in the intensity of donors and acceptors, such as those that occur in FRET. Different approaches for measuring FRET using spectral imaging based on spectral unmixing algorithms have been reported. These methods (Chen et al., 2007; Gut et al., 2004; Neher and Neher, 2004; Raicu et al., 2005; Zimmermann et al., 2002), use lifetime (Neher and Neher, 2004; Raicu et al., 2005), or acceptor photobleaching measurements as calibration procedures (Gut et al., 2004; Raicu et al., 2005; Zimmermann et al., 2002). Chen and coworkers implemented an intensity normalized acceptor cross excitation correction (Chen et al., 2007). Other interesting methods based in spectral unmixing using multiphoton microscopy (Thaler et al., 2005) or spectrofluorometer systems (Wlodarczyk et al., 2008) have been developed. Here, we present a new method for the analysis of FRET based entirely on spectral image acquisition using laser scanning confocal microscopy. We evaluated the performance of lambda FRET (λFRET) using FRET standards, and found that this method is more sensitive and reproducible than acceptor photobleaching and sensitized emission-based methods. The method was applied to both fixed and live intra- and intermolecular FRET studies for the analysis of the in vivo interaction of CD44 and moesin in invasive tumor cells embedded in three-dimensional (3D) collagen matrices, further demonstrating the suitability of λFRET for monitoring molecular interactions in cell biology applications.

MATERIALS AND METHODS

FRET Microscopy and Image Analysis

Raw images for FRET analysis were collected with a Leica SP2 AOBS spectral confocal microscope equipped with a 63 × 1.4 NA oil objective (Leica Microsystems CMS, Mannheim, Germany) by using λ*D*488/λ*A*543 laser lines (for the pairs Alexa 488-Cy3 and GFP-mRFP), or λ*D*458/λ*A*514 laser lines (for the pair CFP-YFP and Cerulean-Venus). λ stacks are acquired by obtaining a λ series of fluorescence images by defining 30 (25-nm wide) detection windows over the range of 465–650 nm, although the number and width of detection windows is configurable depending on the signal strength and speed requirements. Accordingly, the time needed for the acquisition varies depending on the scan format, ranging from around 80–14 s for λ stacks of 30 or 18 fluorescence images respectively using a Leica SP2 microscope. In contrast sensitized emission raw image acquisition takes around 1 s. Standard reference spectra are obtained by exciting the donor and acceptor control samples with the donor excitation wavelengths. The donor excitation wavelength is used to obtain the acceptor reference spectra since it enables the acquisition of the complete λ stack ranging all the detection wavelengths. In λFRET analysis, a donor and acceptor excitation wavelengths are used to obtain one reflection and a λ stack of images. The reflected light intensity is measured from a reflection image obtained by configuring a detection window that matches the excitation wavelength. From each fluorescence image λ stack, intensities are plotted against the median wavelength value of each detection window to obtain the raw spectra (rawS), or reference spectra (refS), depending on whether the images are originated from the FRET or control samples respectively. RawS were analyzed as specified in the Results section. Theoretical derivation of λFRET corrections and efficiency calculation is detailed in Supporting Information Appendices 1 and 2. IDL software (ITT Visual Information Solutions, CO) was used to integrate computerized image analysis functions into a single λFRET algorithm that could be applied to sets of images and time-lapse image series to obtain FRET efficiency images. Processes performed by IDL include the complete λFRET measurement, including spectra interpolation, CAbs, $\frac{R_{\lambda D}}{R_{\lambda A}}$, and E calculations. Acceptor photobleaching and sensitized emission measurements were performed using the algorithm incorporated into the Leica SP2 confocal software (Wouters et al., 2001).

Spectrofluorometric Analysis of Cell Lysates

MDA-MB-231 pelleted cells were lysed with 50 μL of Triton 0.5%, 10 min on ice and centrifuged at 6,000 rpm 5 min. Supernatant was diluted in PBS at a density of 1×10^6 cells/mL. The emission spectrum of fluorescent proteins in the lysate was acquired with Quantamaster Spectrofotometer (Photon Technology International, Birmingham, NJ) and Felix32 software. CFP emission was traced from 460 to 560 nm with excitation at 430 nm and YFP was traced from 500 to 560 nm with excitation at 490 nm. The increment was 5 nm and the integration 1 s. Determination of FRET efficiencies was performed as described in Chen et al. (2005).

DNA Constructs

A YFP-17aa-CFP tandem construct was generated by amplifying CFP from the ECFP-N1 vector and subsequently cloning it into the EYFP-C1 vector (Clontech, Takara Bio, Shiga, Japan) using *Kpn*I and *Bam*HI. The YFP-8aa-CFP tandem was obtained by amplifying CFP from the ECFP-N1 vector using oligonucleotides introducing a GGTGG motif as a linker with *Bsp*EI-*Bam*HI sticky ends using the following synthetic oligonucleotides: forward, 5′-AGATCCG GAGGTACAGGTGGAGGTACCATGGTGAGCAAGGG C-3′; reverse: 5′-CGGGATCCTTACTTGTACAGCTCG TC-3′. The PCR product was cloned into the EYFP-C1 vector. The R16 domain of chicken α-spectrin was kindly provided by Dr. J. Clarke (University of Cambridge, UK) and the immunoglobulin domain of protein G DNA was kindly provided by Dr. F. Blanco (CNIO, Spain). The R16 and B1G domains were amplified without stop codons and cloned into the *Bsp*EI-*Kpn*I restricted YFP-17aa-CFP tandem to generate YFP-R16-CFP and YFP-B1G-CFP respectively. CFP-YFP-YFP and CFP-CFP-YFP fusion constructs were obtained by amplifying YFP and CFP from EYFP-N1 and ECFP-

N1 vectors respectively, and cloning them into YFP-17aa-CFP tandem with *XhoI-EcoRI* restriction sites. A caspase-sensitive FRET probe YFP-LEVD-CFP was generated by amplifying CFP from the ECFP-N1 vector using a forward oligonucleotide containing two caspase cleavage sites, 5′-AGATCCGGAGCACTGGAGGTCG ATGCCCTGGAGGTCGATGGTACCATGGTGAGCAAG GGCGAGGAG-3′ and cloning it into EYFP-C1 with *Bsp*EI-*Bam*HI. The C5V, C17V, and C32V constructs were provided by Dr. Vogel (National Institutes of Health, Bethesda, MD). The standard form of CD44 amplified from cDNA was provided by Dr. T Mizoi (Kumamoto University, Japan) and cloned into mRFP vector [provided by Dr. Tsien (University of California at San Diego] using *Kpn*I–*Sac*I restriction sites. The moesin-GFP construct was provided by Dr. Sánchez-Madrid (Hospital de la Princesa). All constructs were verified by DNA sequencing.

Cell Culture, Transfection, and Collagen Inclusion

Breast adenocarcinoma MDA-MB-231 cells were maintained in DMEM supplemented with 10% FBS. Cell transfection was performed using lipofectamine 2,000 (Invitrogen, Carlsbad, CA) according to the manufacturer's instructions. Twenty-four hours after transfection, cells were trypsinized and mixed with a readily prepared HA-Col I solution (2.4 mg/mL bovine Col I (Vitrogen, PAlo Alto, CA), 1 mg/mL HA (Sigma-Aldrich, St Louis, MO), 1 × RPMI, 19 mM Hepes, 0.19% sodium bicarbonate, 5% FBS, and allowed to polymerize for 2 h at 37°C (3D-Col I) or plated on cover slips either uncoated or coated with HA-Col I.

Immunofluorescence Experiments

FRET-positive controls were performed on MDA-MB-231 cells plated on HA-Col I-coated cover slips, fixed, and stained with HP2/9 mouse antihuman CD44 antibodies, kindly provided by Dr. Sánchez Madrid (Hospital de la Princesa, Spain). Cells were incubated with 5 μg/mL of goat antimouse Alexa 488 (Molecular Probes, Invitrogen) and then with 7.5 μg/mL of donkey antigoat Cy3 (Jackson Inmunoresearch, Westgrove, PA). The CD44-moesin interaction was studied in cells expressing moesin-GFP and CD44-mRFP fixed and stained with rabbit anti-Ezrin/Radixin/Moesin (90/3) and mouse anti-CD44 (HP2/9) antibodies revealed with secondary antirabbit Ab labeled with Alexa 488 (Molecular Probes, Invitrogen) and anti mouse Cy3 labeled Ab (Jackson, Amersham Biosciences, Uppsala, Sweden), respectively.

RESULTS

Rationale of the λFRET Method

A detailed procedure for λFRET data acquisition and analysis for Alexa 488 and Cy3 fluorophores is presented in Figures 1 and 2. Description of symbols can be found in Table 1. First, a series of images acquired at different detection wavelengths (λ stacks) were obtained from samples with only donor or acceptor species generating standard reference spectra (Fig. 2a). These are acquired once for every donor/acceptor pair as part of the precalibration procedure and apply for all subsequent FRET analysis using the same fluorophore combination. For FRET measurement two sets of the reflection image and λ stacks are acquired by exciting the double-labeled sample (FRET sample), with donor-specific (λD, 488) and acceptor-specific (λA, 543) excitation wavelengths and represent raw images (Fig. 2b). Following image background correction, fluorescence intensities are plotted against wavelength to obtain the rawS for every image pixel (Fig. 2b). The spectra datasets obtained with the donor excitation wavelength (raw FRET spectra; $\mathrm{rawS}^{DA}_{\lambda D}$) contain the FRET information, and the spectra acquired by exciting with acceptor specific light (raw direct acceptor spectra; $\mathrm{rawS}^{A}_{\lambda A}$) are used to estimate the cross-excitation contamination component.

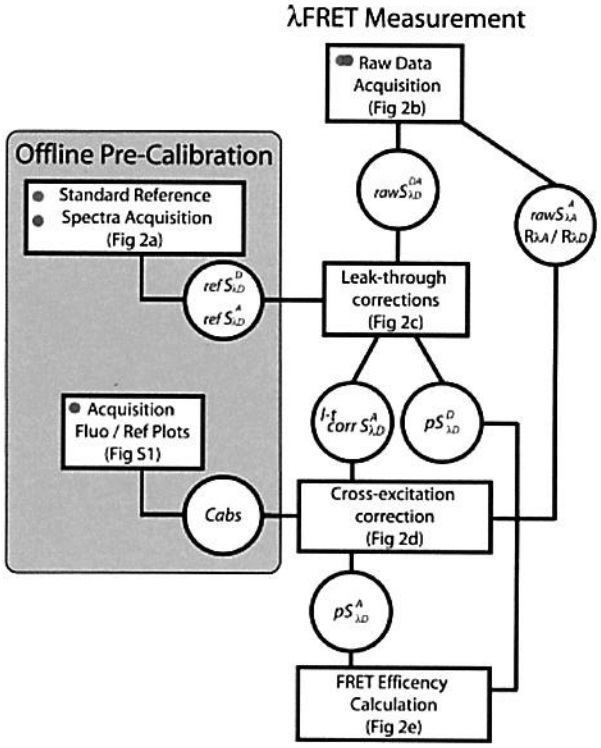

Fig. 1. Flowchart of the λFRET algorithm. Processes involving measurements on acceptor or donor control samples that can be obtained once for a given fluorochrome pair as an offline precalibration procedure are included in the gray box. FRET measurement steps for the processing of data originating from the FRET double labeled sample to calculate the FRET efficiency are shown. More detailed information about these processes can be found at the indicated figures. [Color figure can be viewed in the online issue, which is available at www.interscience.wiley.com.]

Separation of raw FRET spectrum ($\mathrm{rawS}^{DA}_{\lambda D}$) into its donor and acceptor components ($\mathrm{intS}^{A}_{\lambda D}$ and $\mathrm{intS}^{D}_{\lambda D}$ is based on an interpolation procedure that uses reference standard donor and acceptor spectra from single-labeled samples as detailed in Supporting Information Appendix 1 (Fig. 2ci). Leak-through corrections are then carried out by subtracting the fraction of acceptor interpolated emission peak ($\mathrm{intS}^{A}_{\lambda D}$) overlapping donor peak ($\mathrm{intS}^{D}_{\lambda D}$) and vice versa (Figs. 2cii and 2ciii) The leak-through corrected donor spectrum is termed pure donor spectra ($\mathrm{pS}^{D}_{\lambda D}$) because it does not require further

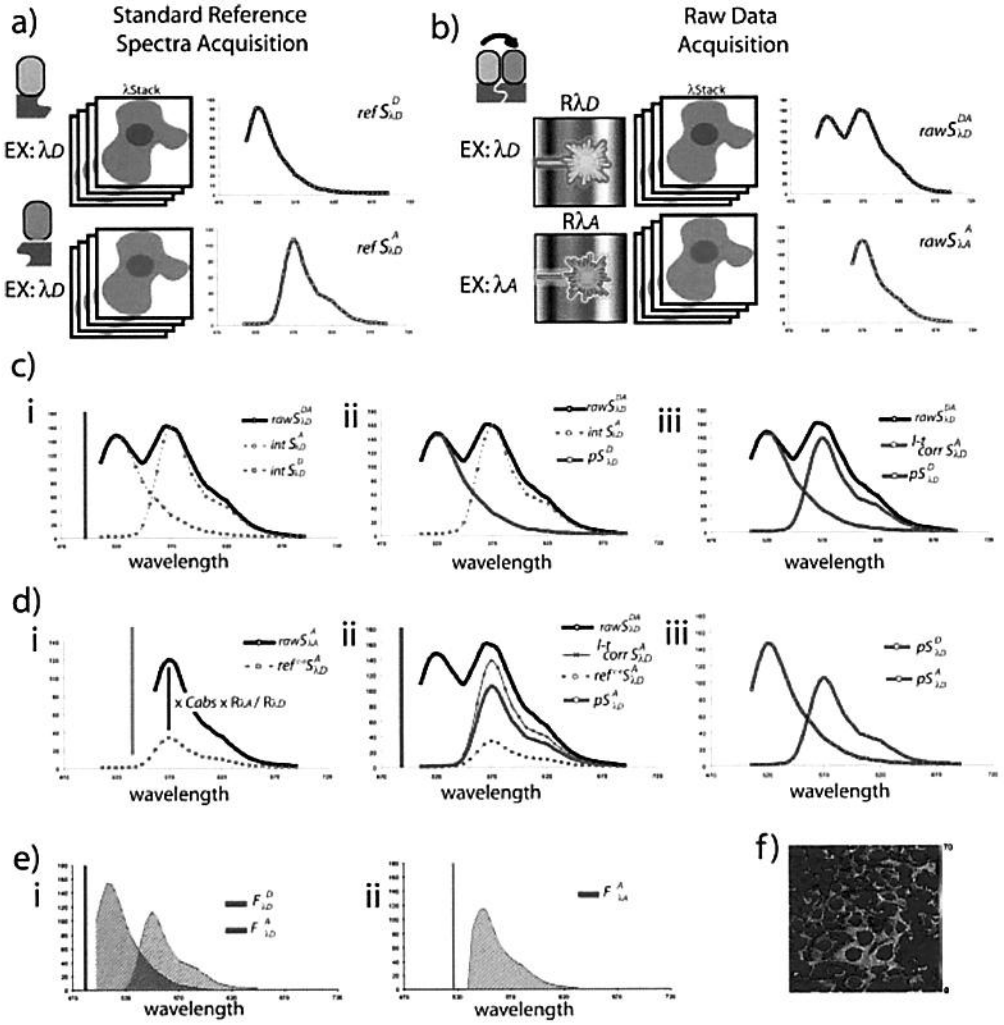

Fig. 2. λFRET data acquisition and analysis procedure. Fixed MDA-MB-231 cells were incubated with mouse anti-CD44 Ab, and then either with secondary goat antimouse Alexa 488, or antimouse Cy3 to obtain control samples (**a**) or with secondary goat antimouse Alexa 488 and with rabbit antigoat Cy3 obtaining the double labeled FRET sample (**b**). (a) λ stacks of 30 fluorescence images were obtained by exciting the control samples with 488 nm laser line (Ex:λ*D*) to render $refS^{A}_{\lambda D}$ and $refS^{D}_{\lambda D}$. (b) One reflection and a spectral series of 30 fluorescence images were obtained by exciting the double labeled sample with 488 nm (Ex:λ*D*) or 543 nm (Ex:λ*A*) laser lines. Representative raw FRET ($rawS^{DA}_{\lambda D}$) and raw direct acceptor emission spectra ($rawS^{A}_{\lambda A}$) are shown. (**c**) The raw FRET spectrum ($rawS^{DA}_{\lambda D}$, solid line) is decomposed into donor and acceptor raw emission peaks ($intS^{D}_{\lambda D}$ and $intS^{A}_{\lambda D}$, dashed lines) by interpolating standard donor and acceptor reference spectra (**i**). Leak-through correction subtracts the percentage of the spectral spillover of the acceptor into the donor (i) and vice versa (**ii**). Preliminary raw FRET spectrum ($rawS^{DA}_{\lambda D}$, solid line) and resultant donor ($pS^{D}_{\lambda D}$ thick solid line) and acceptor leak-through corrected spectra ($^{l\text{-}t}corrS^{A}_{\lambda D}$ thick solid line) are presented (iii). (**d**) The product of raw direct acceptor control spectra ($rawS^{A}_{\lambda A}$, dotted line), the predetermined absorbance constant (C_{Abs}), and reflection intensity ratio ($R_{\lambda D}/R_{\lambda A}$) render reference cross-excitation-corrected spectra ($ref^{c\text{-}e}\ S^{A}_{\lambda D}$, dotted line) i), which is subtracted from the acceptor leak-through-corrected spectra ($^{l\text{-}t}corrS^{A}_{\lambda D}$, thin solid line) to obtain the resultant fully corrected acceptor pure spectra ($pS^{A}_{\lambda D}$, thick solid line) ii). Resultant donor and acceptor pure spectra (thick solid lines) are presented iii). Raw FRET spectra ($rawS^{DA}_{\lambda D}$) is shown with clarity purposes in cii, ciii, and dii graphs. (**e**) Donor directly excited and acceptor sensitized fluorescence intensity values ($F^{D}_{\lambda D}$ and $F^{A}_{\lambda D}$) are calculated from the $pS^{D}_{\lambda D}$ and $pS^{A}_{\lambda D}$ spectral curve integrals (**i**) and acceptor directly excited fluorescence emission intensity value $F^{A}_{\lambda A}$ is calculated from $pS^{A}_{\lambda A}$ curve integral (**ii**). (**f**) The resultant λFRET efficiency image is shown.

corrections. In contrast, the leak-through corrected acceptor spectrum $^{l\text{-}t}corrS^{A}_{\lambda D}$ carries a cross-excitation contamination that needs to be corrected. The cross-excitation contamination component of the FRET spectrum is the amount of acceptor emission excited directly at the donor-specific wavelengths. We have developed a completely novel correction procedure based in imaging the double labeled sample to avoid the variability produced by introducing intensity measurements coming from control single labeled sample. The cross-excitation-correction procedure (Fig. 2d) is based on deriving a cross-excitation reference spectrum as the product of the direct acceptor raw spectrum, the ratio of reflection intensities at the donor and acceptor wavelengths ($R_{\lambda D}/R_{\lambda A}$), both obtained from the FRET double-labeled sample, and the

TABLE 1. Description of symbols

Code	Description	Originated in
$rawS^{DA}_{\lambda D}$	Raw FRET spectra of donor and acceptor emission excited at donor λ	FRET sample
$intS^{D}_{\lambda D}$	Interpolated donor raw emission spectra excited at donor λ	$rawS^{DA}_{\lambda A}$
$intS^{A}_{\lambda D}$	Interpolated acceptor raw emission spectra excited at donor λ	$rawS^{DA}_{\lambda A}$
$rawS^{A}_{\lambda A}$	Raw acceptor emission spectra directly excited at acceptor λ	FRET sample
$refS^{A}_{\lambda D}$	Reference acceptor emission spectra directly excited at donor λ	Control acceptor sample
$refS^{D}_{\lambda D}$	Reference donor emission spectra excited at donor λ	Control donor sample
$^{l-t}corrS^{A}_{\lambda D}$	Leak through corrected acceptor emission spectra excited at donor λ	$intS^{A}_{\lambda D}$
$ref^{c-e}S^{A}_{\lambda D}$	Reference acceptor cross excitation spectra	$rawS^{A}_{\lambda A}$
$pS^{D}_{\lambda D}$	Pure donor emission spectra excited at donor λ (leak-through corrected).	$intS^{D}_{\lambda D}$
$pS^{A}_{\lambda D}$	Pure acceptor emission spectra excited at donor λ (leak-through and cross excitation corrected).	$^{l-t}corrS^{A}_{\lambda D}$
$F^{D}_{\lambda D}$	Donor fluorescence intensity directly excited at donor λ	$pS^{D}_{\lambda D}$
$F^{A}_{\lambda D}$	Acceptor sensitized fluorescence intensity derived from energy transfer.	$pS^{A}_{\lambda D}$
$F^{A}_{\lambda A}$	Acceptor fluorescence intensity directly excited at acceptor λ	$rawS^{A}_{\lambda A}$

Capital Letter: S, spectra; L, incident light intensity; I, raw fluorescence intensity; F, corrected fluorescence intensity; Abs, light absorption; C, constant; R, reflected light intensity; E, FRET efficiency; Q, quantum yield. Super index: *D*, emission at donor wavelength range; *A*, emission at acceptor wavelength range. Sub index: λ*D*, donor-specific excitation wavelength; λ*A*, acceptor-specific excitation wavelength. Prefix: ref^{c-e}, reference for cross-excitation; ref, reference from control sample; $^{l-t}corr$, data corrected for leak-through; raw, raw data; int, interpolated values; p, pure, fully corrected. [Color figure can be viewed in the online issue, which is available at www.interscience.wiley.com.]

acceptor absorbance constant (C_{Abs}) (Fig. 2d) using the following equation:

$$ref^{c-e}S^{A}_{\lambda D} = \frac{R_{\lambda D}}{R_{\lambda A}} \cdot C_{\mathrm{abs}} \cdot rawS^{A}_{\lambda A}$$

(derived in Supp. Info. Appendix 1)

C_{Abs} is calculated by the software once for every donor–acceptor fluorochromes on an acceptor only sample as part of the precalibration procedure and used for cross-excitation correction of subsequent FRET studies. This value correlates linearly the acceptor absorption coefficients at the donor and acceptor laser lines. C_{Abs} calculation is computed as the relationship between the slopes of the fluorescence reflection plots excited at the donor and acceptor wavelengths (Supp. Info., Fig. S1) following:

$$C_{\mathrm{Abs}} = \frac{I^{A}_{\lambda D} \cdot R_{\lambda A}}{I^{A}_{\lambda A} \cdot R_{\lambda D}} \quad \text{(derived in Supp. Info. Appendix 1)}$$

By applying C_{Abs} and ($R_{\lambda D}/R_{\lambda A}$) correction factors, the acceptor emission spectra directly excited at the donor specific wavelength ($ref^{c-e}S^{A}_{\lambda D}$) can be deduced from the raw acceptor spectrum obtained from exciting the FRET sample at the acceptor wavelength ($rawS^{A}_{\lambda A}$) (Fig. 2di), then subtracted from the leak-through corrected acceptor spectrum ($^{l-t}corrS^{A}_{\lambda D}$) to obtain an acceptor pure spectrum ($pS^{A}_{\lambda D}$), (leak-through and cross-excitation corrected) (Fig. 2dii). Both donor and acceptor pure spectra ($pS^{D}_{\lambda D}$ and $pS^{A}_{\lambda D}$) are used for FRET efficiency calculations (Fig. 2diii). The corrected fluorescence intensities from direct excitation of donor $F^{D}_{\lambda D}$, and sensitized acceptor emission $F^{A}_{\lambda D}$ are obtained from pure spectra curve integrals (Fig. 2ei) and used for λFRET efficiency computation following equation:

$$E = \frac{F^{A}_{\lambda D} \cdot Q^{D}/Q^{A}}{F^{D}_{\lambda D} + F^{A}_{\lambda D} \cdot Q^{D}/Q^{A}}$$

(derived in Supp. Info. Appendix 2)

The acceptor direct fluorescence emission intensity calculated as the ($rawS^{A}_{\lambda A}$) curve integral (Fig. 2eii) is used for donor/acceptor ratio calculations (Supp. Info. Appendix 3). The λFRET software developed in-house automatically implements the analysis algorithm that determines E in a pixel-based manner to obtain a FRET efficiency image (Fig. 2f). Systematic and propagation errors in λFRET efficiency calculation were analyzed as detailed in Supporting Information Appendix 4. In a typical experimental analysis, the calculated maximum error value for each spectrum ($\Delta pS^{A}_{\lambda D} = \Delta pS^{D}_{\lambda D}$) was = 5,17 (Supp. Info. Fig. S2). The standard error (SE) propagation was 0.003 for a measured λFRET efficiency value of 0.35.

In summary, λFRET comprises spectral imaging of a FRET sample, and results in a pixel-based composite FRET spectrum which is separated into its donor and acceptor components, and is corrected for leak-through and acceptor cross-excitation using a novel, off-line precalibration procedure. Fully corrected donor and acceptor spectra, termed pure spectra, are used for the pixel-based calculation of λFRET efficiency, which renders an efficiency image.

Validation of λFRET Method Using Tandem Yellow Fluorescent Protein-Cyan Fluorescent Protein Constructs Generated as FRET Standards

To validate the λFRET method, a number of yellow fluorescent protein (YFP)-cyan fluorescent protein (CFP) fusion constructs with variable linker length and stoichiometry were genetically engineered. Tandem YFP-CFP fusions connected through scaffolds differing in length were designed to test λFRET accuracy. R16 domain of chicken brain α-spectrin (R16), and the immunoglobulin binding domain of streptococcal protein G (B1G) for both of which the 3D structures have been solved (Gronenborn et al., 1991; Pascual et al., 1997) (PDB accession numbers 1AJ3 and 1GB1) were used as linkers. According to their rigid structure and with their predicted length of 41 and 25 Å, R16 and B1G standards were expected to render medium and low FRET efficiencies, respectively. We also designed two fusion constructs incorporating short synthetic

flexible peptide linkers of 8 and 17 amino acids (named Ln8aa and Ln17aa, respectively), which were predicted to allow the closest proximity of fluorescent proteins and therefore optimal FRET efficiency. A caspase-sensitive probe, LEVD, consisting on two caspase cleavage sites inserted as a spacer into YFP-CFP fusion construct served as a negative control with fixed stoichiometry when cells where subjected to caspase activating campthotecin (Cpt) apoptotic stimuli. A schematic representation of the different constructs is shown in Figure 3a. To test the λFRET method, we analyzed MDA-MB-231 cells expressing each of these standards, or CFP and YFP coexpressed separately, which served as a negative control of unknown stoichiometry. Raw FRET spectra obtained from Ln17aa, B1G, and R16 constructs by spectral confocal imaging showed marked qualitative differences (Fig. 3b), that translated into significant differences in the λFRET efficiency images (Fig. 3c). Ln8aa and Ln17aa displayed equivalent results (not shown). As expected, the flexible peptide linker (Ln17aa) displayed the highest FRET efficiency value, and B1G or R16 domains displayed lower, but significant, efficiencies according to the length of the linker placed between the fluorescent proteins. These experiments validated λFRET as a method to calculate FRET efficiency that is specific and sensitive to distance variations.

λFRET Performance Evaluation

FRET standards developed herein were used to compare the performance of λFRET with other, well-established FRET-measuring methods based on confocal microscopy. The FRET efficiency values were obtained using λFRET, sensitized emission and acceptor photobleaching methods, as detailed in Supporting information Appendix 2. Analysis was performed in parallel in MDA-MB231 cells expressing either the Ln17aa, B1G, R16, or LEVD fusion constructs treated or not with Cpt, or CFP+YFP expressed separately (Fig. 4a). The λFRET results were consistent with those obtained with acceptor photobleaching method (Fig. 4a). Sensitized emission values resulted more unstable especially at low transfer efficiencies (R16) and negative control (CFP+YFP) (Supp. Info., Fig. S3). Fold induction calculation of the ratio of FRET efficiency obtained for the different FRET standards compared with the negative control (cells expressing LEVD treated with Cpt) represents an evaluation of the capability of the different methods of resolving molecular distances is shown in Supp. Info., Fig. S3). These results showed that, although other methods resolved the different distances of the tandem fusions, λFRET was more sensitive to distance variations (Fig. 3a and Supp. Info., Fig. S3). To further evaluate FRET accuracy, we expressed C5V, C17V, and C32V FRET standards that have been previously characterized (Koushik et al., 2006). The λFRET results obtained with these standards were in good agreement with the reported FRET efficiency values generated by averaging the results of E-FRET, FLIM, and sRET methods (Fig. 4b). These results further validate λFRET method and show clearly its advantage resolving molecular distances.

Intermolecular FRET studies are highly dependent on donor and acceptor concentrations. In order to test applicability of the λFRET method for intermolecular FRET of stoichiometry differing from 1:1, we generated CFP-CFP-YFP and CFP-YFP-YFP fusion constructs (Fig. 4c). λFRET resultant pure fluorescence emission intensities were used to calculate donor acceptor stoichiometry from these constructs following the equation;

$$[D]/[A] = \frac{(F^{A}_{\lambda D}/G) + F^{D}_{\lambda D}}{F^{A}_{\lambda A} \cdot R_{\lambda D}/R_{\lambda A} \cdot k}$$

(derived in Supp. Info. Appendix 3)

This equation is derived as a variation of the method described by Chen et al. (2006). Where G is a proportionality constant that represents the ratio of sensitized acceptor emission to the quenched donor emission and can be determining by analyzing two standard encoding donor acceptor fusion FPs differing widely in FRET efficiency. k is the ratio of donor to acceptor fluorescence for equimolar concentrations in the absence of FRET and can be calculated once the G factor is determined using a 1:1 donor–acceptor fusion construct. As detailed in Supporting Information Appendix 3, $[D]/[A]$, G, and k calculation based in λFRET resultant $F^{A}_{\lambda D}$ and $F^{A}_{\lambda A}$ values was generated from Ln17aa and R16aa standard analysis. The mean, $[D]/[A]$ ratios measured from cells expressing CFP-YFP fusion construct were 1.03 ± 0.12, whereas those obtained for the CFP-CFP-YFP and CFP-YFP-YFP were 2.13 ± 0.5 and 0.56 ± 0.16 respectively, very close to the expected values of 1, 2, and 0.5. Then, we analyzed FRET efficiencies by λFRET, sensitized emission, acceptor photobleaching, and spectrofluorometric methods. λFRET, acceptor photobleaching, and spectrofluorometric methods were proven to be quite stable to changes in the concentration of donor and acceptor (Fig. 4d). λFRET efficiency calculation was almost unaffected by addition of CFP, although it was slightly raised by the extra copy of YFP, most probably due to an increased availability of acceptor, rather than to the variation in the concentration. Accordingly, both acceptor photobleaching and spectrofluorometric methods, which are independent of donor/acceptor concentration, also resulted in an increase in efficiency of CFP-YFP-YFP standards compared with Ln17aa tandem (Fig. 4d), demonstrating it is due to an increase in energy transfer ruling out the possibility of a concentration-dependent error. The sensitized emission method underestimated efficiency at any given variation of stoichiometry (Supp. Info. Fig. S3). To demonstrate advantage of λFRET analyzing donor acceptor pairs with high spectral overlap, we constructed a CFP-Ln17aa-GFP fusion which rendered 32% efficiency, equivalent to its CFP-Ln17aa-YFP counterpart. Sensitized emission clearly underestimated efficiency of CFP-GFP and acceptor photobleaching was found useless for this fluorophore pair since bleaching of acceptor also produced donor fluorescence decay (Fig. 5a). Although autofluorescence can represent a problem with FRET determination, it should not affect the λFRET method, since the pixels that cannot be fitted to a reference spectrum are removed from the subsequent FRET calculation. This was formally demonstrated by analyzing cells expressing Ln17aa tandem bearing highly autofluorescent intracellular spots which did not affect the FRET measurement (Fig. 5b). This analysis demonstrates clearly the robustness of the λFRET method under conditions

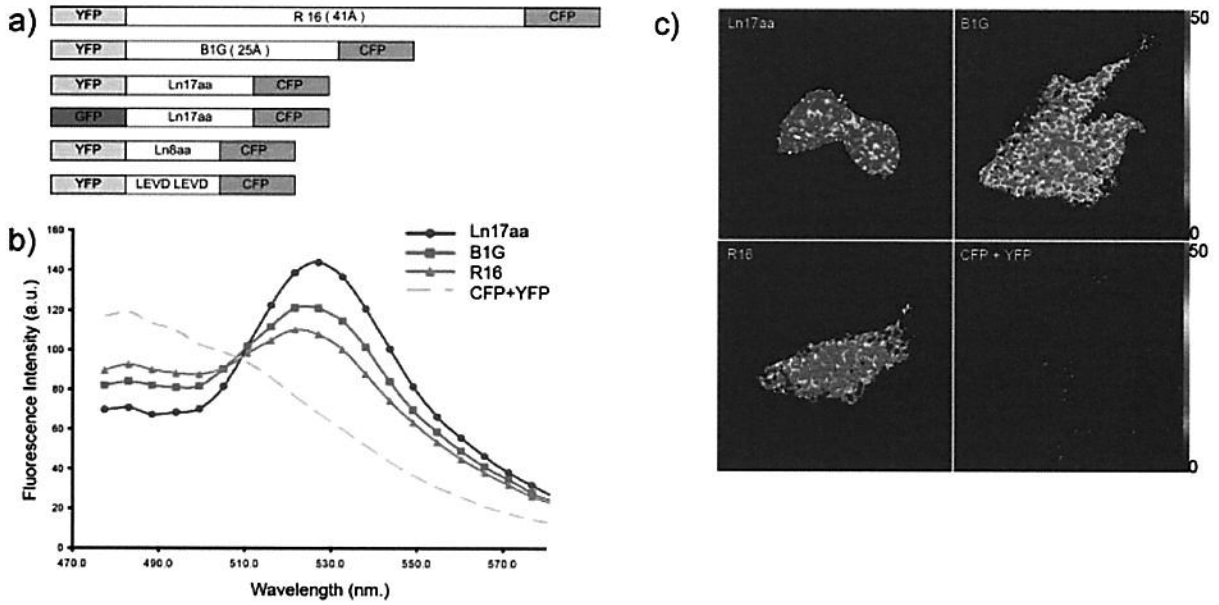

Fig. 3. Validation of the λFRET method with FRET standards. (**a**) Schematic representation of tandem YFP-CFP fusions (R16, B1G, Ln17aa, Ln8aa, and LEVD), and a spectral variant of tandem Ln17aa (GFP-Ln17aa-CFP). (**b**) MDA-MB231 cells were transfected with tandem YFP-CFP constructs (Ln17aa, B1G, and R16) or with YFP and CFP expression vectors (YFP+CFP) used as a negative control. Raw FRET spectra were obtained by spectral confocal imaging upon excitation at 458 nm. (**c**) Representative FRET efficiency pseudocolored images resulting from λFRET analysis of these constructs are shown.

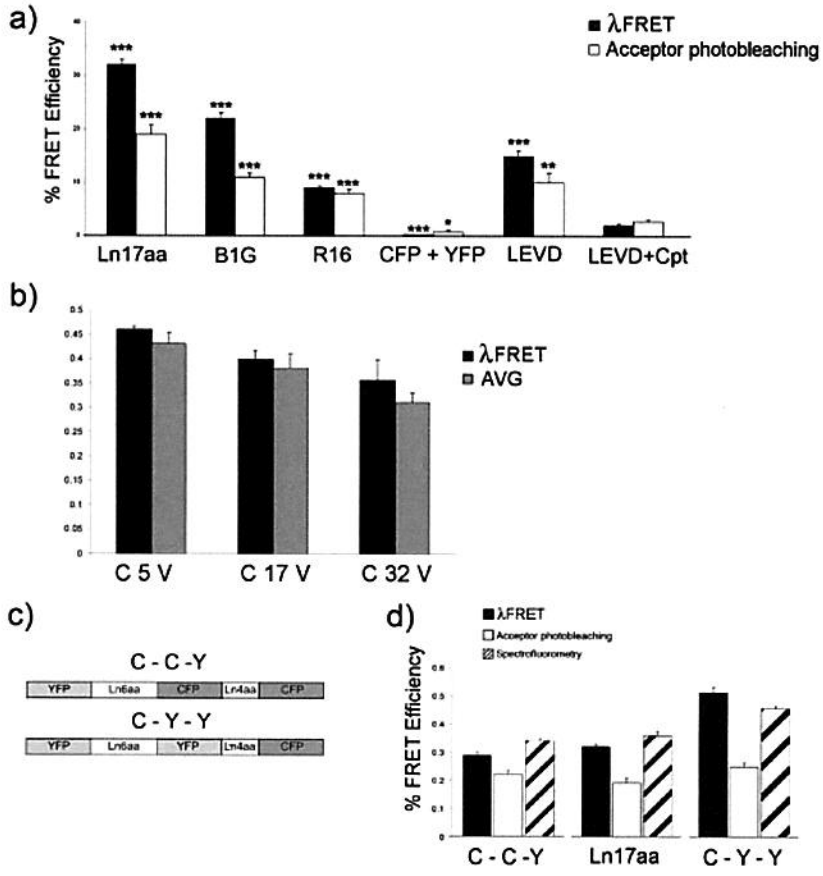

Fig. 4. λFRET comparative evaluation. (**a**) MDA-MB-231 cells were transfected with FRET standards (Ln17aa, B1G, and R16), LEVD, CFP-CFP-YFP, CFP-YFP-YFP, or CFP + YFP. Cells treated or not with 20 μM Cpt for 24 h were analyzed in parallel using λFRET (solid bars), acceptor photobleaching (open bars), or spectrofluorometric methods (dashed bars). The significance of differences between the FRET standard fusion constructs and control (LEVD + Cpt) values was evaluated using Student's *t*-test; $P < 0.05$ was considered significant ($^*P < 0.05$, $^{**}P < 0.01$, $^{***}P < 0.001$). (**b**) MDA-MB-231 cells were transfected with FRET standards C5V, C17V, and C32V. FRET efficiency was quantified using λFRET (solid bars) and compared with the average of FRET measurements described for these standards in Koushik et al. (2006) (gray bars). (**c**) Schematic representation of constructs with variable stoichiometry, YFP-CFP-CFP (Y-C-C) and YFP-YFP-CFP (Y-Y-C). (**d**) MDA-MB-231 cells transfected with Y-C-C, Y-Y-C, and Ln17aa were analyzed in parallel using λFRET (solid bars), acceptor photobleaching (open bars), or spectrofluorometric methods (dashed bars). (a–d) Bar diagrams represent FRET efficiency quantification calculated from 75 cells of five independent experiments, expressed as the mean ± SE.

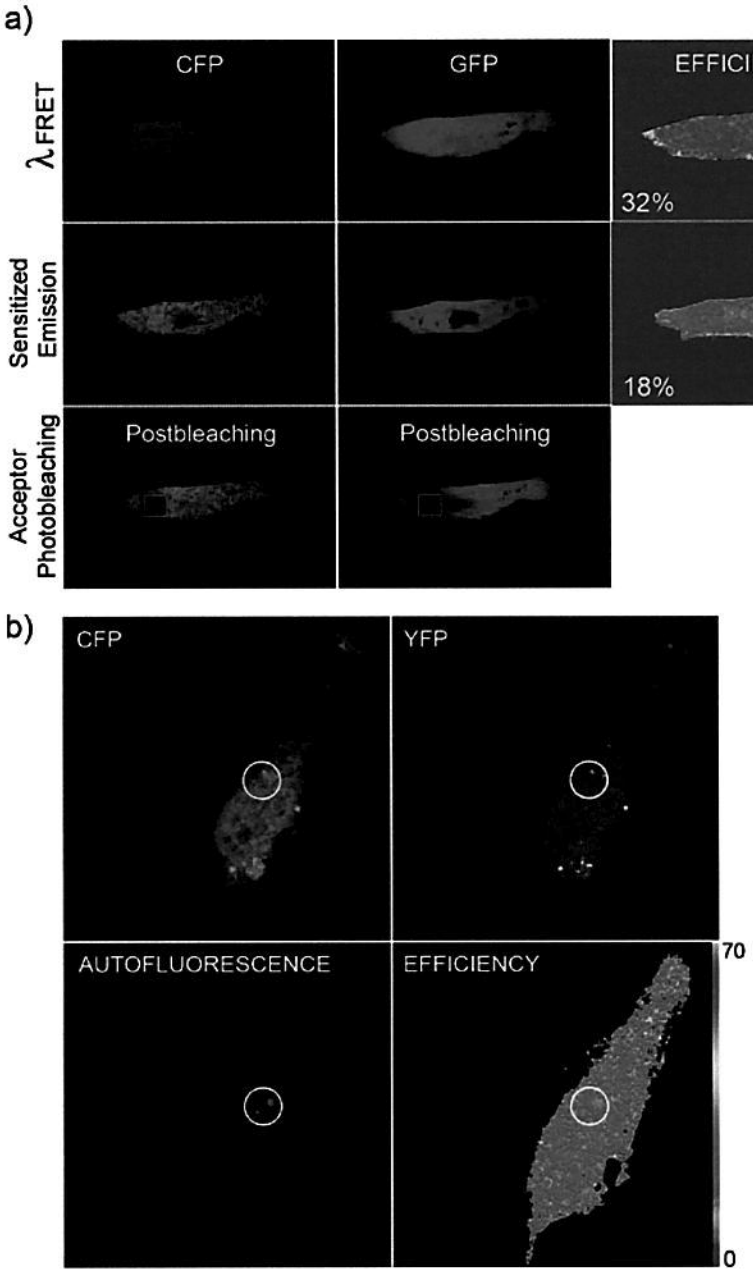

Fig. 5. Fluorochrome spectral overlap and autofluorescence does not affect λFRET efficiency measurement. (a) MDA-MB-231 cells expressing CFP-Ln17aa-GFP were analyzed. CFP, GFP, and efficiency images obtained using λFRET, sensitized emission, and acceptor photobleaching methods are shown. Measured FRET efficiency values are indicated. MDA-MB-231 cells expressing CFP-Ln17aa-YFP FRET standard were analyzed by λFRET. Expression of CFP (blue), YFP (yellow), autofluorescent granules (red), and FRET efficiency pseudocoloured image are shown. Circle highlights localization of autofluorescent granules.

of donor/acceptor stoichiometry differing from 1:1, high fluorochrome spectral overlap and cellular autofluorescence. Altogether, these results show that the performance was better for λFRET than for acceptor photobleaching and sensitized emission methods.

Application of λFRET to Fixed and Live Cell Intermolecular FRET Imaging

Interaction of CD44 and moesin has been previously studied using conventional biochemical approaches and by FRET studies monitored by FLIM microscopy (Legg et al., 2002; Yonemura et al., 1998), and therefore is a good candidate to test performance of λFRET for studying typically weak physiological molecular interactions. With this aim we analyzed breast carcinoma MDA-MB-231 cells expressing, moesin-GFP and CD44-monomeric red fluorescent protein (mRFP), or CD44-GFP and caveolin-mRFP used as a negative control. As expected, both acceptor photobleaching and λFRET methods rendered positive FRET efficiency values for CD44–moesin but not for CD44–caveolin analysis (Fig. 6a). To demonstrate applicability of λFRET for monitoring dynamic interactions in live cell studies, we

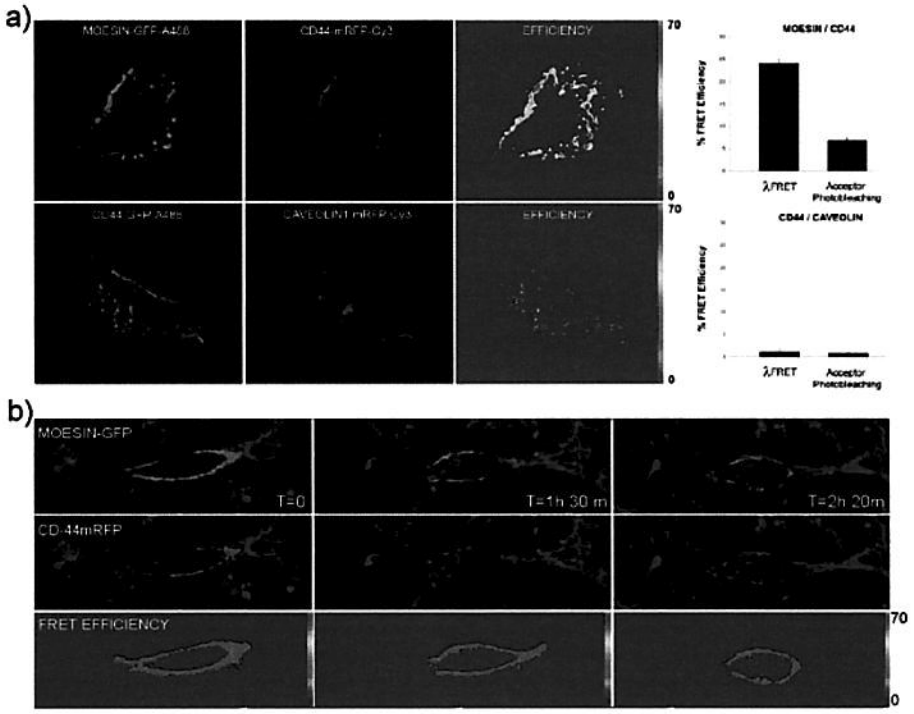

Fig. 6. λFRET study of CD44–moesin interaction in fixed and live cell studies of tumor cell invasion. (**a**) MDA-MB-231 cells were cotransfected with moesin-GFP and CD44-mRFP, or CD44-GFP and caveolin-mRFP, and plated on HA-Col I coated cover slips. Cells were fixed and stained with anti-CD44, anti-ERM, or anticaveolin antibodies revealed with secondary antibodies labeled with Alexa 488 or Cy3. Representative donor (green) and acceptor (red) fluorescence and pseudocolored FRET efficiency images are shown. Bar diagrams represent mean FRET efficiency values calculated using λFRET or acceptor photobleaching methods from 12 cells in three independent experiments. (**b**) MDA-MB-231 cells cotransfected with CD44-mRFP and moesin-GFP were embedded in 3D collagen matrices. Representative GFP (green) and mRFP (red) fluorescence, overlaid on the reflection image showing collagen fibers (blue) and pseudocolored λFRET efficiency images depicted from the video sequence at the times indicated are shown.

imaged MDA-MB-231 cells migrating into 3D collagen type-I matrices. A series of λFRET efficiency images depict the sequence of steps of tumor cell invasion where the interaction of CD44 and moesin at the cell surface was detected (Fig. 6b). Although most CD44 and moesin accumulated at the cell poles, this was not translated into higher FRET values at these areas. Regardless of the variations in fluorescence intensity of donor (moesin) and acceptor (CD44), FRET values remained constant during the migratory process, further demonstrating that FRET calculation is independent of the donor/acceptor concentration (Fig. 6b). Together, these studies demonstrate that λFRET is a suitable method for studying intermolecular interactions in both fixed and live cell imaging experiments.

DISCUSSION

Because of limitation of methods for monitoring FRET in living cells using standard, commercially available confocal microscopes, we sought to develop a procedure based on spectral analysis, to take advantage of its unique capability to detect complex changes associated with FRET. The method needed to be sensitive and nondestructive to be able to detect the typically weak physiological interactions in live cell studies. We herein describe the new λFRET method, which we validated with structurally characterized FRET standards of variable lengths that were designed and constructed for this purpose demonstrating λFRET outstanding performance compared with other well-established FRET methods.

Spectral imaging based linear unmixing algorithms are very useful for quantifying individual fluorophores from a combined emission spectra but fail when FRET is occurring because it takes into account spectral bleed-through contaminations but not for acceptor cross-excitation derived artifacts (Thaler et al., 2005). Different approaches for measuring FRET using spectral imaging based unmixing algorithms have been reported (Gut et al., 2004; Neher and Neher, 2004; Raicu et al., 2005; Thaler et al., 2005; Zimmermann et al., 2002). To overcome these linear unmixing limitations, these spectral methods introduce lifetime (Neher and Neher, 2004; Raicu et al., 2005) or acceptor photobleaching measurements (Gut et al., 2004; Raicu et al., 2005; Zimmermann et al., 2002) to the FRET calculations. Thaler and coworkers have implemented sRET, that uses a spectral unmixing formula which incorporates the emission by the donor and acceptor as result of direct excitation as well as emission from the acceptor resulting from FRET that is solved to obtain donor and acceptor concentrations as well as FRET efficiency values (Thaler et al., 2005). The relative contri-

bution of each fluorochrome and an excitation wavelength-dependent constant k are determined from spectral datasets coming from samples with only donor or acceptor at equal concentrations excited at two different wavelengths. Similarly to sRET, another spectral FRET method, lux-FRET, is also based on spectral unmixing two wavelength excitation measurements (Wlodarczyk et al., 2008) and uses four calibration spectra from donor and acceptor samples imaged at two excitation wavelengths. Interestingly, lux-FRET calculations take into consideration the contributions of unpaired donor and acceptor fluorophores and the influence of incomplete labeling of the interacting partners. The recently described spectral psFRET method (Chen et al., 2007) utilizes an spectral unmixing approach to calculate FRET efficiency based in confocal microscopy. psFRET removes acceptor cross-excitation at donor wavelengths using an algorithm that matches fluorescence intensity levels of control cells that express acceptor alone, to the sample that express both donor and acceptor fluorochromes.

Unlike any other previously described FRET measuring method, λFRET introduces a novel correction procedure based on the use of reflection images to normalize for different radiation light intensities. In addition, the λFRET method decomposes the FRET spectra into its donor and acceptor components using an interpolation procedure different from linear unmixing. This interpolation procedure has the disadvantage of being more susceptible to a reduction in the number of spectral detection windows compared to linear unmixing. However, the strength of our interpolation procedure is that it enables us to eliminate the pixels that cannot be fitted to the reference spectra for subsequent FRET calculation making this method independent of autofluorescence (Fig. 5b) or other sources of unspecific FRET distortions. In addition, it enables us to separate highly overlapping spectra, as was demonstrated here for the CFP GFP pair (Fig. 5a). Although we use a high number of overlapping detection windows in our λ stacks, the accuracy of λFRET efficiency calculations did not suffer from reducing the spectral channels to 18.

The two widely used methods of FRET quantification by confocal microscopy imaging are acceptor photobleaching and sensitized emission. Acceptor photobleaching is a simple, reproducible and concentration independent method that has a number of limitations, mainly because it is destructive and therefore unsuitable for live cell experiments, and because it gives information only about the bleached area. The FRET efficiency results were in good agreement with those obtained with acceptor photobleaching method, although the latter tended to give lower efficiency values. Taking into account that FRET efficiency is an instrument- and methodology-independent parameter, the values measured using these two methods should be equivalent. The differences in the absolute values observed herein are consistent with other studies which have reported that the acceptor photobleaching method renders an underestimation of the FRET efficiency which is reated to incomplete acceptor photobleaching and undesired donor photobleaching caused errors (Berney and Danuser, 2003; Karpova et al., 2003; Raicu et al., 2005).

Sensitized emission based methods are popular for live FRET imaging in laboratories that don't have access to FLIM microscopy. However, our sensitized emission results were unstable and not consistent at low transfer efficiencies (R16) and in the negative (CFP + YFP) control with unknown stoichiometry. This is most probably due to the use of confocal imaging, which raises a number of complications that do not apply to wide field imaging, like the use of two independent detectors and excitation laser lines. Some correction schemes for these errors have been developed (van Rheenen et al., 2004), although they were not accounted for in this work because we used the SP2 Leica confocal software which does not correct them. This may be the main cause of the herein registered inconsistencies. The λFRET method is not subject to these errors since it uses only one detector and the ratio of reflection intensities corrects for differences of incident light power coming from the use of different excitation laser lines. Another source of problems inherent to this method is the underlying assumption that the amount of leak through is independent of the absolute intensity of the fluorophores and can be calibrated off-line in samples containing only donor or acceptor at arbitrary concentrations. Confocal systems based in photomultiplier (PMTs) which have a limited linear range of detection, are more likely to render inconsistencies resulting from assuming a linear dependence of the spectral bleed-through component on the fluorescence intensity. Others have implemented interesting correction procedures to avoid instability problems of the sensitized emission method coming from this source (van Rheenen et al., 2004; Elangovan et al., 2003). However, these errors should, in principle not affect the λFRET method since the spectral leak-through corrections are not based in absolute intensities, or determining the contribution of fluorophore as in spectral unmixing, but is based in spectral curve interpolation. Additionally, λFRET inherently takes into account exclusively the values coming from the PMTs linear range of detection and therefore should avoid errors coming from this source.

λFRET is similar to sensitized emission based methods since both rely on the measurement of acceptor fluorescence emission due to energy transfer, although λFRET has a number of advantages. (1) Because it is based not on absolute fluorescence intensities, but on the analysis of spectral curve integrals, this method should be more robust to photobleaching induced by repeated analysis of the sample in live cell experiments. λFRET also avoids the variability resulting from the nonlinear relation between the leak-through and absolute fluorescence intensities. (2) λFRET monitors simultaneous changes in donor and acceptor fluorescence and is therefore more reliable. The measurements should in principle be less susceptible to artifacts caused by nonspecific quenchers such as formaldehide fixation, which has been shown to quench Cerulean and Venus FPs differentially and affect donor acceptor ratios dramatically (Chen et al., 2006). (3) Imaging of control single-labeled samples for spectral bleed-through corrections can be performed once for any given fluorochrome pair and microscope setup as a precalibration procedure, and used for subsequent FRET measurements. This avoids additional causes of

variability in the efficiency calculation because of inconsistencies in donor and acceptor concentrations between the control and the double-labeled sample. (4) Although detector PMT settings (gain and offset) must be kept constant, the normalization of excitation light intensity inherent to the λFRET method permits free tuning of the excitation light intensity, allowing a good signal-to-noise ratio imaging that avoids saturation effects. In addition, the normalization for the excitation light intensity corrects for variability because of laser instability in live cell studies. (5) Its ability to unmix spectrally overlapping signals, as demonstrated by the analysis of CFP-GFP tandem, allows high flexibility in the choice of FRET probes. Our comparison of methods using FRET standards tested in parallel demonstrated superior specificity, sensitivity, and stability of λFRET than both acceptor photobleaching and sensitized emission. (6) λFRET can be used to measure donor acceptor ratios. Moreover, λFRET was found to be quite stable at different donor/acceptor concentrations and independent of fluorochrome spectral overlap and autofluorescence. The main drawback of λFRET is that spectral imaging is time consuming and therefore not suitable for analyzing rapid live cell processes. However, commercially available spectral confocal instruments can work at an extremely high scan speed, and spectral acquisitions can be acquired simultaneously with an array of detectors working in parallel, so time is not a practical limitation. There are still some advantages of FLIM over λFRET, since the fluorescence lifetime is absolutely insensitive to variations in concentration and excitation intensity and no spectral bleed-through correction is needed, factors that relatively limit intensity based steady state measurements. However FLIM has some drawbacks since it requires expensive equipment and skilled manipulation and due to its sensitivity to environmental changes (Wallrabe and Periasamy, 2005).

In summary, the new λFRET method was useful for different combinations of donor–acceptor pairs (Alexa 488-Cy3, CFP-YFP, Cerulean-Venus, CFP-GFP and GFP-mRFP), intramolecular FRET of stoichiometric (1:1) donor–acceptor concentrations, and intermolecular FRET of unknown stoichiometry. More importantly, λFRET was successfully applied to analyzing CD44-moesin interaction in fixed and live cells during tumor cell invasion, demonstrating its outstanding capabilities.

ACKNOWLEDGMENTS

The authors thank Dr. F Blanco for help with design of FRET standards, F Camas, Dr. JF Poyatos, Dr. R Diaz, and Dr. J. Rivera for their helpful advice, and A Piera and Dr. J Llopis for their advice and critical reading of the manuscript. Dr. Mizoi, Dr. Sánchez-Madrid, Dr. Blanco, Dr. Clarke, and Dr. Tsien are acknowledged for providing us with reagents.

REFERENCES

Berney C, Danuser G. 2003. FRET or no FRET: A quantitative comparison. Biophys J 84:3992–4010.

Chen H, Cohen DM, Choudhury DM, Kioka N, Craig SW. 2005. Spatial distribution and functional significance of activated vinculin in living cells. J Cell Biol 169:459–470.

Chen Y, Mauldin JP, Day RN, Periasamy A. 2007. Characterization of spectral FRET imaging microscopy for monitoring nuclear protein interactions. J Microsc 228:139–152.

Chen H, Puhl HL, Koushik SV, Vogel SS, Ikeda SR. 2006. Measurement of FRET efficiency and ratio of donor to acceptor concentration in living cells. Biophys J 95:L39–L41.

Elangovan M, Wallrabe H, Chen Y, Day RN, Barroso M, Periasamy A. 2003. Characterization of one- and two-photon excitation fluorescence resonance energy transfer microscopy. Methods 29:58–73.

Förster T. 1965. Delocalized excitation and excitation transfer. In: Sinanoglu O, editor. Modern quantum chemistry, Vol. 3. New York: Academic Press Inc., pp 93–137.

Gronenborn AM, Filpula DR, Essig NZ, Achari A, Whitlow M, Wingfield PT, Clore GM. 1991. A novel, highly stable fold of the immunoglobulin binding domain of streptococcal protein G. Science 253:657–661.

Gu Y, Di WL, Kelsell DP, Zicha D. 2004. Quantitative fluorescence resonance energy transfer (FRET) measurement with acceptor photobleaching and spectral unmixing. J Microsc 215:162–173.

Jares-Erijman EA, Jovin TM. 2003. FRET imaging. Nat Biotechnol 21:1387–1395.

Karpova TS, Baumann CT, He L, Wu X, Grammer A, Lipsky P, Hager GL, McNally JG. 2003. Fluorescence resonance energy transfer from cyan to yellow fluorescent protein detected by acceptor photobleaching using confocal microscopy and a single laser. J Microsc 209:56–70.

Koushik SV, Chen H, Thaler C, Puhl HL, III, Vogel SS. 2006. Cerulean, venus, and venusY67C FRET reference standards. Biophys J 91:L99–L101.

Legg JW, Lewis CA, Parsons M, Ng T, Isacke CM. 2002. A novel PKC-regulated mechanism controls CD44 ezrin association and directional cell motility. Nat Cell Biol 4:399–407.

Lerner JM, Zucker RM. 2004. Calibration and validation of confocal spectral imaging systems. Cytometry A 62:8–34.

Neher RA, Neher E. 2004. Applying spectral fingerprinting to the analysis of FRET images. Microsc Res Tech 64:185–195.

Pascual J, Pfuhl M, Walther D, Saraste M, Nilges M. 1997. Solution structure of the spectrin repeat: A left-handed antiparallel triple-helical coiled-coil. J Mol Biol 273:740–751.

Raicu V, Jansma DB, Miller RJ, Friesen JD. 2005. Protein interaction quantified in vivo by spectrally resolved fluorescence resonance energy transfer. Biochem J 385:265–277.

Thaler C, Koushik SV, Blank PS, Vogel SS. 2005. Quantitative multiphoton spectral imaging and its use for measuring resonance energy transfer. Biophys J 89:2736–2749.

van Rheenen J, Langeslag M, Jalink K. 2004. Correcting confocal acquisition to optimize imaging of fluorescence resonance energy transfer by sensitized emission. Biophys J 86:2517–2529.

Wallrabe H, Periasamy A. 2005. Imaging protein molecules using FRET and FLIM microscopy. Curr Opin Biotechnol 16:19–27.

Wlodarczyk J, Woehler A, Kobe F, Ponimaskin E, Zeug A, Neher E. 2008. Analysis of FRET signals in the presence of free donors and acceptors. Biophys J 94:986–1000.

Wouters FS, Verveer PJ, Bastiaens PI. 2001. Imaging biochemistry inside cells. Trends Cell Biol 11:203–211.

Yonemura S, Hirao M, Doi Y, Takahashi N, Kondo T, Tsukita S. 1998. Ezrin/radixin/moesin (ERM) proteins bind to a positively charged amino acid cluster in the juxta-membrane cytoplasmic domain of CD44. CD43, and ICAM-2. J Cell Biol 140:885–895.

Zhang J, Campbell RE, Ting AY, Tsien RY. 2002. Creating new fluorescent probes for cell biology. Nat Rev Mol Cell Biol 3:906–918.

Zimmermann T, Rietdorf J, Pepperkok R. 2003. Spectral imaging and its applications in live cell microscopy. FEBS Lett 546:87–92.

Zimmermann T, Rietdorf J, Girod A, Georget V, Pepperkok R. 2002. Spectral imaging and linear un-mixing enables improved FRET efficiency with a novel GFP2-YFP FRET pair. FEBS Lett 531:245–249.